2019

Boundary conditions and Berry phase in magnetic nanostructures

A. Ullah

B. Balamurugan

W. Zhang

D. J. Sellmyer

R. Skomski

Boundary conditions and Berry phase in magnetic nanostructures

Cite as: AIP Advances **9**, 125049 (2019); https://doi.org/10.1063/1.5130477
Submitted: 09 October 2019 . Accepted: 12 November 2019 . Published Online: 27 December 2019

A. Ullah, B. Balamurugan, W. Zhang, D. J. Sellmyer, and R. Skomski

Boundary conditions and Berry phase in magnetic nanostructures

Cite as: AIP Advances 9, 125049 (2019); doi: 10.1063/1.5130477
Presented: 8 November 2019 • Submitted: 9 October 2019 •
Accepted: 12 November 2019 • Published Online: 27 December 2019

A. Ullah, B. Balamurugan, W. Zhang, D. J. Sellmyer, and R. Skomski[a)]

AFFILIATIONS

Department of Physics and Astronomy and Nebraska Center for Materials and Nanoscience, University of Nebraska, Lincoln, Nebraska 68588, USA

Note: This paper was presented at the 64th Annual Conference on Magnetism and Magnetic Materials.
[a)]R. Skomski, rskomski@neb.rr.com

ABSTRACT

The effect of micromagnetic boundary conditions on the Berry curvature and topological Hall effect in granular nanostructures is investigated by model calculations. Both free surfaces and grain boundaries between interacting particles or grains affect the spin structure. The Dzyaloshinskii-Moriya interactions yield corrections to the Erdmann-Weierstrass boundary conditions, but the Berry curvature remains an exclusive functional of the local spin structure, which greatly simplifies the treatment of nanostructures. An explicit example is a model nanostructure with cylindrical symmetry whose spin structure is described by Bessel function and which yields a mean-field-type Hall-effect contribution that can be related to magnetic-force-microscopy images.

I. INTRODUCTION

The topological Hall effect (THE) reflects the Berry phase accumulated by conduction electrons exchange-interacting with spin structures $\boldsymbol{S}_i = \boldsymbol{S}(\boldsymbol{R}_i)$.[3,21] To yield a nonzero emergent magnetic field (Berry-phase curvature), the local spin structures must be noncoplanar, $\boldsymbol{S}_i \cdot (\boldsymbol{S}_j \times \boldsymbol{S}_k) \neq 0$. Such spin structures are often associated with Dzyaloshinskii-Moriya (DM) interactions,[1–5,13,22] but micromagnetic spin structures such as magnetic bubbles are also noncoplanar.[6,7,14] This paper deals with granular magnetic nanostructures, such as interacting nanoparticles and melt-spun alloys. The spin structures in these systems are well-known to be noncollinear, and the question arises whether and how this noncollinearity translates into a THE. One example is thin films made from ensembles of MnSi nanoparticle having average sizes between 9.7 and 17.7 nm.[12] Ensembles of metallic magnetic nanoparticles can be made conducting through compaction or embedding in a conductive matrix.

Our emphasis is on grain-boundary effects, which reflect that the Euler-Lagrange equations for $\boldsymbol{S}(\boldsymbol{r})$ are of the type $\partial E/\partial \boldsymbol{S} - \nabla \cdot (\partial E/\partial \nabla \boldsymbol{S}) = 0$, where E is the micromagnetic (free) energy.[9] In the absence of DM interactions, the only $\nabla \boldsymbol{S}$-dependent term in the energy density is $A\,(\nabla \boldsymbol{S})^2$, where $A(\boldsymbol{r})$ is the local exchange stiffness. The corresponding term in the Euler-Lagrange equations is $\nabla(A \nabla \boldsymbol{S})$, which reduces to $A\nabla^2 \boldsymbol{S}$ for chemically homogeneous systems.[18] For boundaries between two phases I and II, the Euler-Lagrange equations yield the Erdmann-Weierstrass boundary conditions[10]

$$A_I \frac{\partial \boldsymbol{S}_I}{\partial r_s} = A_{II} \frac{\partial \boldsymbol{S}_{II}}{\partial rs} \tag{1}$$

where $\partial \boldsymbol{S}/\partial r_s$ is the derivative with respect to the spatial coordinate perpendicular to the surface. Free surfaces (interfaces between magnetic materials and vacuum) have $A_{II} = 0$ and Eq. (1) reduces to $\partial \boldsymbol{S}/\partial r_s = 0$ at the surface. The Dzyaloshinskii-Moriya interaction is linear in $\nabla \boldsymbol{S}$ and therefore yields an additional term in the Euler-Lagrange equations.[15,23] This term needs to be specified for each point group, and there is generally no one-to-one correspondence between broken inversion symmetry and the existence of DM interactions.[20] For example, inverse cubic Heusler coumpounds (point group T_d) have broken inversion symmetry but no DM interactions.

In this paper, we investigate how Berry-phase curvature and topological Hall effect depend on the physical nature and geometry of the grain boundaries. We review DM interactions in cylindrical nanoparticles of crystals belonging to the point groups C_{nv} and show that these nanoparticles yield a simple micromagnetic mean-field description of skyrmions in granular nanostructures.

II. CYLINDRICAL NANOPARTICLES WITH FREE SURFACES

The starting point for the discussion of DM boundary conditions is the micromagnetic free energy[8]

$$E = \int \left[A(\nabla \boldsymbol{s})^2 - K s_z{}^2 - \mu_o M_s H_z s_z + \varepsilon_{DM}\right] dV \quad (2)$$

where $\boldsymbol{s} = \boldsymbol{S}(\boldsymbol{r})/|S|$ is the normalized magnetization. The second and third terms in this equation are the anisotropy and Zeemann energies, respectively,[18,19,25] whereas the last term describes the DM interactions. Note that the approach in this section follows the treatment by Rohart and Thiaville,[15] which ignores magnetostatic self-interactions. Mathematically, this neglect makes sense, because boundary conditions refer to quasi-local short-range interactions of the gradient type. By contrast, magnetostatic interactions are long-range and correspond to magnetic charges at surfaces, and the effect of these charges is macroscopic. Magnetostatic interactions can be ignored on very small length scales, where the interatomic exchange (A) dominates.[18] While a comprehensive description of magnetostatic effects in systems with DM interactions is a challenge to future research, Sect. III solves the problem on an approximate level.

The last term in Eq. (2), which describes the Dzyaloshinskii-Moriya interactions, is often expressed in terms of Lifshitz invariants[1,2,16]

$$L_{ij}^k = S_i \frac{\partial s_j}{\partial x_k} - S_j \frac{\partial s_i}{\partial x_k} \quad (3)$$

The exact form of DM interaction is determined by the point-group symmetry of the compound.[20] Inversion symmetry, polarity, and chirality the a canonical division into centrosymmetric crystals, noncentrosymmetric crystals without DM interactions, noncentrosymmetric crystals with DM interactions but no spin spirals, and noncentrosymmetric crystals supporting both DM interactions and helical spin structures.[20]

For the polar point groups C_{nv}, which describe a number of bulk and thin-film structures, $\varepsilon_{DM} = D(L_{xz}^x + L_{yz}^y)$. Explicitly,

$$\varepsilon_{DM} = D(s_z \nabla \cdot \boldsymbol{s} - \boldsymbol{s} \cdot \nabla s_z) \quad (4)$$

B20-ordered materials such as MnSi belong to the point group T, where $\varepsilon_{DM} = D\,\boldsymbol{s}\cdot(\nabla \times \boldsymbol{s})$.

The steady-state spin structure is obtained as

$$\delta E/\delta \boldsymbol{s} = -\mu_B \int_V \boldsymbol{s}(\boldsymbol{r}) \times \boldsymbol{B}_{eff} dV + \int_S \boldsymbol{\Gamma}_s dS \quad (5)$$

where the effective field

$$\boldsymbol{B}_{eff} = 2A\nabla^2 \boldsymbol{s} + 2K s_z \boldsymbol{e}_z + \mu_o H \boldsymbol{e}_z + 2D(\boldsymbol{e}_z \nabla \cdot \boldsymbol{s} - \nabla(\boldsymbol{s} \cdot \boldsymbol{e}_z)) \quad (6)$$

For the point groups C_{nv}, the surface term is

$$\boldsymbol{\Gamma}_s = 2A\boldsymbol{s} \times \frac{\partial \mathbf{s}}{\partial rs} - D(s_z \boldsymbol{s} \times \boldsymbol{n} - \boldsymbol{s} \cdot \boldsymbol{n}(\boldsymbol{s} \times \boldsymbol{e}_z)) \quad (7)$$

The emergent field includes both radial and angular contributions, both depending on the real-structure morphology. We consider a particle with cylindrical symmetry around $\boldsymbol{e}_z$ and a z-independent magnetization. The magnetization is therefore

$$\boldsymbol{s}(\boldsymbol{r}) = \sin\theta(\rho)\cos\phi \boldsymbol{e}_x + \sin\theta(\rho)\sin\phi \boldsymbol{e}_y + \cos\theta(\rho)\boldsymbol{e}_z \quad (8)$$

where θ is the magnetization angle with respect to the z-axis, ρ and ϕ are cylindrical real-space coordinates, and $\partial \boldsymbol{s}/\partial r_s = \partial \boldsymbol{s}/\partial \rho$. The cross product in Eq. (7) ensures the conservation of the normalization ($\boldsymbol{s}^2 = 1$).

The equilibrium (steady-state) condition, $\boldsymbol{s}(\boldsymbol{r}) \times \boldsymbol{B}_{eff} = 0$, is complemented by the boundary condition[15]

$$\frac{\partial \boldsymbol{s}}{\partial r_s} = \frac{D}{2A} \boldsymbol{s} \times (\boldsymbol{n} \times \boldsymbol{e}_z) \quad (9)$$

which follows from Eq. (7). In these coordinates, the Euler-Lagrange equation

$$2A\left(\frac{\partial^2 \theta}{\partial \rho^2} + \frac{\partial \theta}{\rho \partial \rho} - \frac{1}{\rho^2}\sin\theta\cos\theta\right) - 2K\sin\theta\cos\theta - \mu_o H M_s \sin\theta - \frac{2D}{\rho}\sin^2\theta = 0 \quad (10)$$

and the boundary condition is $\partial\theta/\partial\rho = D/2A$ at $\rho = R$. For $D = 0$, Eq. (9) reduces to the Erdmann-Weierstrass boundary conditions, $\partial \boldsymbol{s}/\partial \rho = 0$ in cylindrical coordinates. For $D \neq 0$, the boundary condition yields a rotation (tilting) of the magnetization $\boldsymbol{s}$ in the plane between $\boldsymbol{e}_z$ and the cylindrical surface normal.

The behavior of small particles is dominated by the interatomic exchange, so that $\theta(\rho)$ is small. Linearization of Eq. (10) the causes the bulk DM contribution to vanish and a reverse field causes $\theta(\rho)$ to become unstable. The corresponding magnetization mode $\theta(\rho)$ is described by the Bessel equation

$$\xi^2 \frac{d^2\theta}{d\xi^2} + \xi \frac{d\theta}{d\xi} + \xi^2\theta - \theta = 0 \quad (11)$$

where $\xi = \rho/\rho_o$ and $\rho_o = [A/(\mu_o|H|M_s - K)]^{1/2}$. Equation (11) corresponds to the boundary condition $d\theta/d\xi = D/2\gamma_o$, where $\gamma_o = [A(\mu_o|H|M_s - K)]^{1/2}$. Note that ρ_o and γ_o may be considered as wall-width and wall-energy parameters for the present problem.

The solutions of Eq. (11) are Bessel functions $J_1(\xi)$. In the absence of DM interactions, $dJ_1/d\xi = 0$, which corresponds to the first maximum of $J_1(\xi)$, which is at $\xi = R/\rho_o = 1.841$ (dashed curve

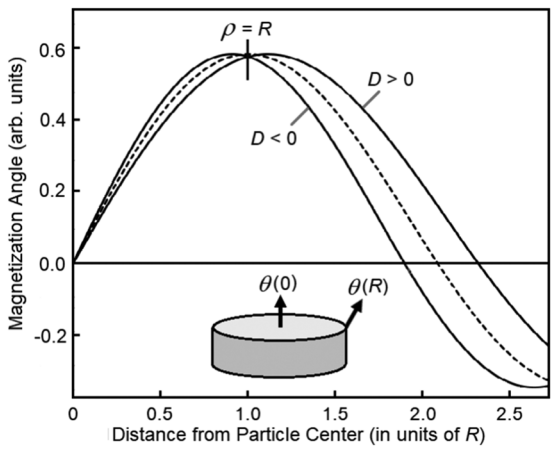

FIG. 1. Magnetization angle $\theta(\rho) \sim J_1(\rho/\rho_o)$ in a model nanoparticle with cylindrical symmetry.

in Fig. 1). The length ρ_o depends on the magnetic field, so that $R = 1.841\ \rho_o$ is an implicit condition for skyrmion formation. The field scales as $H \sim A/R^2$, that is, small nanoparticles require high reversed fields to exhibit the skyrmionic instability shown in Fig. 1.

The inclusion of the DM interaction means that $J_1(\xi)$ is no longer a maximum at R. Depending on the sign of D, the curve contracts or expands until the boundary condition is satisfied (solid curves in Fig. 1). The relative strength of the boundary effect is given by the dimensionless but field-dependent ratio D/γ_o. Figure 1 highlights an important aspect of nanoscale skyrmionics, namely that spins structures need to be geometrically accommodated subject to the appropriate boundary conditions. For example, spin spirals in B20 materials have a certain intrinsic wavelength, and when the nanostructural feature size is smaller than this wavelength, then the spirals are suppressed or change their micromagnetic characteristics. This has been observed in Ref. 12.

III. SKYRMION DENSITY IN EMBEDDED NANOPARTICLES

Conduction electrons traveling through magnetic nanostructures and adiabatically interacting with localized spins Si acquire a Berry phase whose curvature corresponds to an emergent magnetic field and to a corresponding contribution to the Hall effect.[17] This contribution is known as the topological Hall effect (THE), although it is not quantized. The Berry curvature is proportional to $\boldsymbol{S}_i \cdot (\boldsymbol{S}_j \times \boldsymbol{S}_k)$ and, in a continuum approximation, given by the skyrmion density which is[3,11,21]

$$\Phi = \frac{1}{4\pi} \boldsymbol{s} \cdot \left(\frac{\partial \boldsymbol{s}}{\partial x} \times \frac{\partial \boldsymbol{s}}{\partial y} \right) \tag{12}$$

The corresponding contribution to the anomalous Hall effect, known as the topological Hall effect, is obtained by integration over Eq. (12). For fully developed skyrmions, this integral is quantized, $Q = \pm 1$, depending on the magnetization in the core of the skyrmions.

Figure 2 shows some spin structures of interest in the present context. A detailed analysis reveals that the configurations (a) and (b) yield exactly the same Berry curvature,[3] so that we can empoley Eq. (8) for this calculation.

For the assumed cylindrical symmetry, $4\pi\rho\Phi(\rho) = \sin\theta \mathrm{d}\theta/\mathrm{d}\rho$ and the skyrmion number $Q = \int \Phi \mathrm{d}x\mathrm{d}y$ becomes

$$Q = \frac{1}{2}(1 - \cos\theta_o) \tag{13}$$

where $\theta_o = \theta(R)$. This equation is remarkable, because it depends on the magnetization angle θ at $\rho = R$ but not on the derivative $\partial\theta/\partial\rho$, in spite of $\partial\theta/\partial\rho = D/2A$. In other words, the DM interaction affects θ in Eq. (11) but does not explicitly appear in the expressions for Berry phase, emergent field, and topological Hall effect. Note that Q in Eq. (11) is generally noninteger, so that the Hall-effect should better be called 'fractional' or 'partial' topological Hall effect. This includes merons,[24] Fig. 2(d), where $Q = \pm 1/2$. Realistic spin structures in polycrystalline materials, schematically shown in Fig. 2(d), tend to exhibit noninteger values $-1 < Q < +1$, depending on the magnetization history. Furthermore, strong magnetization gradients near the particle's surface violate Berry's adiabacity condition, a consideration more important in nanoparticulate systems than in ordinary skyrmionic thin films.

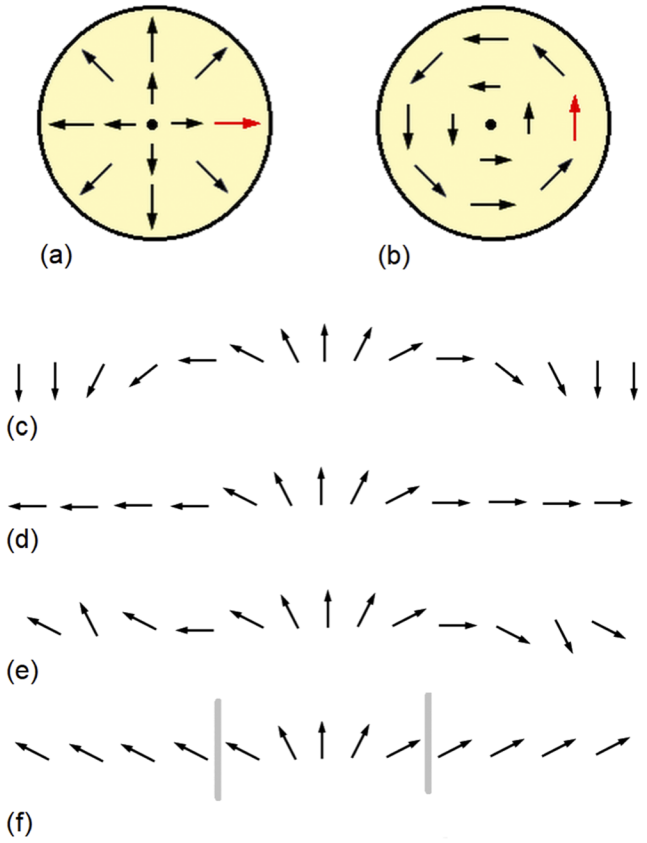

FIG. 2. Nanogranular spin structures: (a) Néel-type skyrmion, (b) Bloch-type skyrmion, (c) fully developed bubble or chiral skyrmion, $\theta_o = 180°$, (d) meron, $\theta_o = 90°$, (e) polycrystalline magnet or 'bubble soup', and (f) micromagnetic mean-field approximation. Spins structures of the type (e) frequently occur in nanoparticular magnets, produced for example by melt spinning.

The exact determination of spin structures such as that in Fig. 2(d) and the evaluation of the corresponding skyrmion density Φ are demanding, even in the absence of DM interactions. A highly simplified model is to embed a single grain of radius R in a mean-field environment, as in Fig. 2(f). Equation (13) shows that the topological number Q is given by the magnetization angle $\theta_o = \theta(R)$ near the grain boundary, symbolized by the two vertical bars in (f). In contrast to the free surfaces of Sect. II, where the spin structure is determined by $\partial\theta/\partial\rho = D/2A$ at $\rho = R$, the present angle θ_o reflect grain misalignment and grain-boundary interactions, as discussed for example in Ref. 18 (Sect. 4.5). The angle is system-specific and reflects a number of structural and magnetic parameters, such as grain size, grain misalignment, magnetic anisotropy, bulk and grain-boundary exchange, and DM interactions. Since Eq. (12) is quadratic in the spatial derivatives, the THE per grain scales very roughly as $1/R^2$, which consistent with available experiments.[12]

The angle θ_o has a relatively simple experimental interpretation in terms of magnetic-force microscopy (MFM). Assuming that the magnetization in the grains is perpendicular to the surface, θ_o corresponds to the MFM contrast: the more pronounced the

contrast, the larger θ_o. Note that θ_o is actually the z-component of the magnetization, further substantiating the connection to the MFM contrast.

It is important to keep in mind that completely random spin structures do not yield a net Hall-effect contribution, because they create emergent magnetic fields that average to zero. Such random spin structures can be created, for example, by thermal demagnetization. To yield a nonzero net contribution, the magnetic regions of one spin direction must be embedded in a background of opposite (or different) magnetization. Such spin structures can be created through the application of an external magnetic field, as exemplified by bubble skyrmion in perfect thin films. The model of Fig. 2(f) includes this key feature in a semiquantitative manner. Note that features sizes in granular nanostructures can be very small, down to a very few nanometers, although such small skyrmions tend to have very low mobilities.

IV. CONCLUSIONS

Depending on the magnetization history, granular nanostructures accumulate a Berry phase that translates into an emergent magnetic field and yields a topological Hall effect. The effect depends on the crystal structure, particle size, grain orientation, and grain-boundary morphology and is, in general, noninteger. Much of the involved physics is included by considering a mean-field model with cylindrical symmetry. Dzyaloshinskii-Moriya interaction terms yields corrections to the Erdmann-Weierstrass boundary conditions that govern the grain-boundary behavior of particulate nanostructures made from inversion-symmetric crystals. However, these corrections affect the topological Hall effect only indirectly, by modifying the local spin structure.

ACKNOWLEDGMENTS

This research is supported by DOE/BES (DE-FG02-04ER46152) and NCMN.

REFERENCES

[1] A. N. Bogdanov and D. A. Yablonskii, "Thermodynamically stable "vortices" in magnetically ordered crystals. The mixed state of magnets," Sov. Phys. JETP **68**, 101 (1989).
[2] A. Bogdanov and A. Hubert, "Thermodynamically stable magnetic vortex states in magnetic crystals," J. Magn. Magn. Matter. **138**, 255 (1994).
[3] S. Seki and M. Mochizuki, *Skyrmions in Magnetic Materials* (Springer International, Cham, 2016).
[4] U. K. Rößler, A. N. Bogdanov, and C. P. fleiderer, "Spontaneous skyrmion ground states in magnetic metals," Nature **442**, 797 (2006).
[5] R. Becker and W. Döring, *Ferromagnetismus* (Springer, Berlin, 1939).
[6] Y. S. Lin, J. Grundy, and E. A. Giess, "Bubble domains in magnetostatically coupled garnet films," Appl. Phys. Lett. **23**, 485 (1973).
[7] T. Garel and S. Doniach, "Phase transitions with spontaneous modulation-the dipolar Ising ferromagnet," Phys. Rev. B **26**, 325 (1982).
[8] P. Bak and M. H. Jensen, "Theory of helical magnetic structures and phase transitions in MnSi and FeGe," J. Phys. C **13**, L881 (1980).
[9] J. Miltat, *Applied Magnetism* (Kluwer, Amsterdam, 1994), p. 221.
[10] R. Skomski, *Simple Models of Magnetism* (University Press, Oxford, 2008).
[11] G. Volovik, "Linear momentum in ferromagnets," J. Phys. C **20**, L87 (1987).
[12] B. Das, B. Balasubramanian, R. Skomski, P. Mukherjee, S. R. Valloppilly, G. C. Hadjipanayis, and D. J. Sellmyer, "Effect of size confinement on skyrmionic properties of MnSi nanomagnets," Nanoscale **10**, 9504 (2018).
[13] A. Fert, V. Cros, and J. Sampaio, "Skyrmions on the track," Nat. Nanotech. **8**, 152–156 (2013).
[14] B. A. Ivanov, V. A. Stephanovich, and A. A. Zhmudskii, "Magnetic vortices: The microscopic analogs of magnetic bubbles," J. Magn. Magn. Matter. **88**, 116–120 (1990).
[15] S. Rohart and A. Thiaville, "Skyrmion confinement in ultrathin film nanostructures in the presence of Dzyaloshinskii-Moriya interaction," Phys. Rev. B **88**, 184422 (2013).
[16] A. O. Leonov, T. L. Monchesky, N. Romming, A. Kubetzka, A. N. Bogdanov, and R. Wiesendanger, "The properties of isolated chiral skyrmions in thin magnetic films," New J. Phys. **18**, 065003 (2016).
[17] M. V. Berry, "Quantal phase factors accompanying adiabatic changes," Proc. R. Soc. Lond. **392**, 45 (1984).
[18] R. Skomski, "Nanomagnetics," J. Phys.: Condens. Matter **15**, R841–R896 (2003).
[19] W. F. Brown, *Micromagnetics* (Wiley, New York, 1963).
[20] A. Ullah, B. Balamurugan, W. Zhang, S. Valloppilly, X.-Z. Li, R. Pahari, L.-P. Yue, A. Sokolov, D. J. Sellmyer, and R. Skomski, "Crystal structure and Dzyaloshinskii–Moriya micromagnetics," IEEE Trans. Magn. **55**, 7100305 (2019).
[21] D. Xiao, M.-Ch. Chang, and Q. Niu, "Berry phase effects on electronic properties," Rev. Mod. Phys. **82**, 1959–2007 (2010).
[22] U. Güngördü, R. Nepal, O. A. Tretiakov, K. Belashchenko, and A. A. Kovalev, "Stability of skyrmion lattices and symmetries of quasi-two-dimensional chiral magnets," Phys. Rev. B **93**, 064428 (2016).
[23] K. M. D. Hals and K. Everschor-Sitte, "New boundary-driven twist states in systems with broken spatial inversion symmetry," Phys. Rev. Lett. **119**, 127203 (2017).
[24] X. Yu, W. Koshibae, Y. Tokunaga, K. Shibata, Y. Taguchi, N. Nagaosa, and Y. Tokura, "Transformation between meron and skyrmion topological spin textures in a chiral magnet," Nature **564**, 95 (2018).
[25] "Perspective in Theoretical Physics, The collected Papers of E. M. Lifshitz," 1992, Pages 51–65.